Research Article | Vol. 9, No. 12 | 1 Dec 2018 | BIOMEDICAL OPTICS EXPRESS 6425
Biomedical Optics EXPRESS

Characterizing the stratum corneum structure, barrier function, and chemical content of human skin with coherent Raman scattering imaging

SAM OSSEIRAN,[1,2] JOMER DELA CRUZ,[3] SINYOUNG JEONG,[1] HEQUN WANG,[1] CHRISTINA FTHENAKIS,[3] AND CONOR L. EVANS[1,*]

[1] *Wellman Center for Photomedicine, Harvard Medical School, Massachusetts General Hospital, 149 13th Street, Charlestown, MA 02129, USA*
[2] *Harvard-MIT Division of Health Sciences and Technology, 77 Massachusetts Avenue E25-518, Cambridge, MA 02139, USA*
[3] *Basic Science Research Division, The Estée Lauder Companies Inc., 155 Pinelawn Road, Melville, NY 11747, USA*
[*] *evans.conor@mgh.harvard.edu*

Abstract: The most superficial layer of the epidermis, the stratum corneum, plays a crucial role in retaining hydration; if its structure or composition is compromised, dry skin may result as a consequence of poor water retention. Dry skin is typically treated with topical application of humectant agents that attract water into the skin. Corneometry, the industry standard for measuring skin hydration, works by assessing the bulk electrical properties of skin. However, this technique samples a large volume of tissue and thus does not resolve the biochemical changes that occur at the cellular level that may underlie mechanisms of dry skin. These limitations can be addressed using coherent Raman scattering (CRS) microscopy to probe the intrinsic vibrational modes of chemical groups such as lipids and water. In the present study, *ex vivo* human skin explants undergoing dehydration and humectant-induced rehydration were measured via CRS imaging and corneometry. Corneometry data and chemically specific images were obtained from the stratum corneum of each patient sample at each timepoint. The resulting data was statistically analyzed using linear mixed effect model regression analysis. The cellular imaging data revealed water loss in the stratum corneum during dehydration that was correlated with corneometer readings. Interestingly, the imaging data and corneometer readings show differences under the experimental rehydration conditions. The rehydration results suggest that hydration restored by the humectant agents may not be retained by the corneocytes in the *ex vivo* model system. Given the complementary nature of corneometry, a bulk assessment tool, and CRS microscopy, a modality with subcellular resolution implemented here in an en-face tissue imaging setup, these techniques can be used to measure uptake and efficacy of topical compounds in order to better understand their mode of action and improve therapeutic applications.

1. Introduction

The particular functions of skin beyond its role as an interface are diverse and include thermal insulation and regulation [1], defense against foreign pathogens [2], touch-based sensation [3], vitamin D production [4], and prevention of water loss [5, 6]. These roles are dependent on the skin's unique structure and composition, of which the epidermis serves as the outermost selectively permeable barrier that interfaces with the environment.

The epidermis is itself a multilayered structure. The deepest cell layer consists of the stratum basale which underlies the stratum spinosum, followed by the stratum granulosum, and finally followed by the stratum corneum at the skin's surface. Depending on anatomical site, the stratum corneum typically ranges in thickness from 10 to 30 layers of enucleated cells known as

#345793 https://doi.org/10.1364/BOE.9.006425
Journal © 2018 Received 14 Sep 2018; revised 7 Nov 2018; accepted 14 Nov 2018; published 26 Nov 2018

Biomedical Optics EXPRESS

corneocytes and is the primary source of the skin's barrier function [7]. This is accomplished through the structural organization of these cells, which are stacked like protein-rich bricks glued together by a lipid-rich ceramide mortar [8]. The biochemical compositions of both the intracellular and extracellular spaces of the stratum corneum thus play important roles in the skin's barrier function and maintaining hydration.

The stratum corneum can be compromised by a wide variety of factors, both internal and external. Internal perturbations include abnormal enzyme activity, a decrease in natural moisturizing factors, and reductions in stratum corneum water content. These chemical changes can all contribute to a decrease in corneodesmolysis, where the rivet-like proteinaceous complexes that bind neighboring corneocytes together ultimately remain intact rather than undergoing enzyme-driven breakdown, resulting in the formation of powdery flakes at the skin surface. In contrast, external factors such as a dry environment can lead to the gradual dehydration of epidermal layers starting with the stratum corneum. As the deeper layers of the epidermis dehydrate, various inflammatory mediators are progressively released which induce keratinocyte proliferation and disruption of epidermal differentiation. This cascade can ultimately lead to a haphazard synthesis of inadequately structured extracellular matrix elements and hampers the natural barrier function of healthy stratum corneum [6, 9, 10].

The management of dry skin is most commonly achieved using topical agents such as cosmetic moisturizers due to their humectant properties [11, 12]. These compounds, including glycerin and hyaluronic acid, tend to draw and retain water due to their abundant hydroxyl groups and can also influence the phase of the extracellular lipid matrix under dry environmental conditions [13]. Glycerin, for example, favors an appropriately fluid lamellar arrangement of extracellular lipids rather than the solid crystalline phase that tends to form under dry conditions [10, 14].

In order to quantitatively monitor skin hydration, conventional methods based on the measurement of skin electrical properties have been developed and validated. One such industry standard involves the use of a corneometer, a device equipped with a pen-sized handheld probe that is gently pressed onto the skin surface to measure hydration based on the capacitance of the skin itself [15]. Given the high dielectric constant of water under standard ambient conditions, its capacitive properties can be probed for non-invasive inferences of skin hydration. Despite its status as a commercial standard, recent studies have identified sources of small but significant experimental variation in corneometry measurements. One study in particular reported a measurement dependence on the contact pressure applied between the probe and the skin, with increasing pressure resulting in overestimated hydration values [16]. The same group later found intra-sample variability in cases where hydration levels approached saturation, suggesting a decrease in probe sensitivity at the upper limits of hydration [17]. Despite these rather modest sources of variability, corneometry has been widely used in the validation and efficacy testing of cosmetic products and topical drug formulations as well as in occupational health studies [15, 18–22].

While corneometry is a simple, rapid, and effective method for the indirect assessment of skin hydration via capacitance measurements, it is inherently limited to point-based acquisitions over a bulk surface area of approximately 1 cm^2. Because of this, corneometry lacks the sub-cellular spatial resolution needed to identify differences between intracellular versus extracellular hydration and it cannot be used to distinguish the hydration of the various layers and sublayers that constitute human skin [17]. Such information would be useful in assessing and validating treatment strategies by offering spatial information at the cellular scale in a depth-resolved manner. With such specificity, it would be possible to identify the problematic anatomical component requiring treatment (e.g. decreased water retention within corneocyte cell bodies, altered lipid composition of the extracellular matrix), in addition to monitoring the effects of the treatment strategy over time. Dermatological investigations that would otherwise require such levels of contextual detail are technologically limited to destructive sampling techniques such as histology or cryo-scanning electron microscopy [23].

Biomedical Optics EXPRESS

As of now, a critical niche remains unaddressed for assessing skin hydration, structure, and composition in a non-invasive and non-destructive manner with subcellular 3D resolution on living tissues. A potential solution to this problem lies within the non-linear optical imaging modalities that have seen increasing use over the past few decades along with the significant advances in endogenous molecular imaging [24–30]. In particular, coherent Raman scattering (CRS) imaging techniques have become a valuable tool in biomedical research by enabling the visualization of specific chemical groups via contrast based on molecular vibrational signatures [31–33]. Of these techniques, coherent anti-Stokes Raman scattering (CARS) and stimulated Raman scattering (SRS) are two complementary CRS techniques that can be readily used to visualize and quantify both the structure and the chemical composition of skin. Moreover, these optical processes occur simultaneously; it follows that an appropriate microscopy setup allows for simultaneous CARS and SRS imaging.

In this manuscript, we report on the parallel use of both CRS microscopy and corneometry to characterize the structure, barrier function, and chemical content of human *ex vivo* skin samples undergoing dehydration and humectant-induced rehydration. In addition to the bulk hydration assessment offered by corneometry, CRS image stacks of the stratum corneum in *ex vivo* skin explants were acquired to examine the distribution of lipid, protein, and water content by probing their molecular vibrational signatures in two separate experimental contexts designed to determine the morphological and chemical imaging metrics that best explain skin hydration.

2. Materials and methods

2.1. Tissue culture and processing

Human skin samples were obtained from discarded tissues resulting from elective patient surgeries in compliance with the institutional review board of Massachusetts General Hospital (MGH IRB protocol #2015P001267). Upon receiving the skin samples, they were immediately trimmed to remove the subcutaneous fat, and subsequently cut into square pieces approximately 1 to 2 cm^2 in size. The skin samples were then placed on a nutritive gel bed consisting of complete cell medium supplemented with 2% agarose and placed in an incubator at 37°C with 5% atmospheric CO_2 and 95% relative humidity. Tissue samples were utilized within three days of collection in all cases. Prior to imaging, skin samples were visually inspected for any signs of tissue contamination or loss of integrity. Next, the stratum corneum was microscopically inspected before the first imaging timepoint to ensure that both corneocytes and their extracellular matrix were indeed visible. With this routine methodology in place, any discrepancy between specimens was deemed due to inter-patient variability rather than potential tissue degradation following harvesting.

2.2. Corneometer measurements

Skin hydration state was measured on *ex vivo* human skin explants using a corneometer (Corneometer CM 825, Courage+Khazaka Electronic GmbH, Cologne, Germany) according to the manufacturer's instructions. For each measurement, the probe was applied to the skin which then outputs a readout in arbitrary units ranging from 0 to 120. Prior work has served to classify the corneometer readouts obtained from 349 volunteers, where values below 30 indicate very dry skin; measurements ranging from 30 to 40 correspond to dry skin; and values above 40 are considered normal [15]. It is worth noting, however, that these classifications were determined based on data acquired from intact patient skin; the cutoffs between very dry, dry, and normal skin for *ex vivo* human skin explants that have been maintained in an incubator at 37°C with high humidity are likely to differ.

Biomedical Optics EXPRESS

2.3. CRS microscopy

CRS imaging was performed using a dual-output femtosecond pulsed laser source (Insight DeepSee, Spectra-Physics, Santa Clara, CA). One output is widely tunable from 680 to 1300 nm and is used as the pump beam in all CRS experiments, while the other output, fixed at 1040 nm, is used as the Stokes beam. Imaging lipids requires tuning the pump beam to 803 nm in order to probe the symmetric CH_2 stretching vibrational mode at 2845 cm^{-1}, which generates an anti-Stokes signal at 654 nm. Proteins can be probed at a slightly higher energy using a pump wavelength of 796 nm to collect the 645 nm anti-Stokes light, where the CH_3 stretching vibration at 2950 cm^{-1} has been associated with protein signatures. Finally, the OH vibrational stretching mode at 3220 cm^{-1} can be probed by tuning the pump beam to 779 nm, generating anti-Stokes light at 623 nm. The laser beams were combined using a dichroic mirror and routed to the input port of a commercial inverted microscope (FV1000, Olympus, Tokyo, Japan), where imaging was performed using a 1.20 NA objective (UPLSAPO 60XW, Olympus, Tokyo, Japan). Laser powers were maintained below 40 mW at the output of the microscope objective for all skin imaging experiments. CARS detection was achieved using a photomultiplier tube (H7422PA-50, Hamamatsu Photonics, Hamamatsu City, Japan) with appropriate optical filters for detecting each respective anti-Stokes signal in an epi-configuration. For SRS, the Stokes beam intensity was modulated using an electro-optic modulator (EO-AM-R-20-C2, Thorlabs, Newton, NJ) driven at 20 MHz. The detector consisted of a commercial system comprised of a photodiode coupled to a lock-in amplifier (Lock-In Amplifier, APE GmbH, Berlin, Germany) placed downstream of the sample in a trans-configuration.

2.4. Image analysis

Three-dimensional CRS image stacks of the stratum corneum under both hydrated and dehydrated conditions were acquired from the skin surface down to a depth of 15 μm at 1-μm intervals along the depth axis. The vibrational bands of lipids, proteins, and water were probed using both CARS and SRS imaging modalities, resulting in a total of 6 image stacks per imaging area, per timepoint, per treatment condition. Each image stack was then inspected visually and the most superficial slice containing clearly delineated corneocytes — i.e. the topmost slice underlying the keratin layer — was used for all subsequent image analysis. Each corneocyte image set was then processed using FIJI image processing software in order to manually segment corneocytes from the lipid SRS image and generate one region of interest (ROI) per corneocyte within a given field of view. The lipid channel was selected for manual segmentation due to the high contrast between the extracellular and intracellular chemical composition. Once all cells in the field of view were identified, the region of the image encompassing all the identified cells was also selected as an ROI itself. The cell ROIs were then subtracted from this region, resulting in a single ROI that can be used to analyze the extracellular space within the stratum corneum.

The ROIs are then all imported into Matlab (Mathworks, Natick, MA), where a custom image analysis routine applies the segmented masks to the imaging data from all 6 channels, allowing for average measurements of water, lipid, and protein content to be computed for each individual cell within a field of view, in addition to the extracellular space. The algorithm uses the ROI data to perform morphological analysis, where metrics such as cell diameter, perimeter, circularity, and nearest neighbor distances are computed. Applying the ROIs to the imaging data results in a variety of metrics that can be extracted beyond water, lipid, and protein content. Ratios can be computed to compare signals from intracellular and extracellular spaces, or to compare the content of one compound (e.g. lipid) to another (e.g. water) within a given ROI. In total, the image analysis routing returns 35 morphological and compositional metrics per imaging field of view, which are then subjected to statistical analysis using linear regression models to identify trends and correlation between the imaging metrics and the corneometer measurements.

Biomedical Optics EXPRESS

2.5. Skin explant dehydration

In order to investigate the dynamics of skin dehydration using CRS imaging, two sets of skin samples were used, where both samples were processed and maintained in an incubator as previously described in order to reach a steady state of hydration. The skin samples were then both removed from the incubator, whereupon skin hydration was measured using the corneometer and CRS imaging was performed on both sets. Next, one sample was maintained on the nutritive gel bed in order to preserve hydration; the other was left on a plastic dish under ambient atmospheric conditions (22°C, 24% relative humidity) to facilitate dehydration. Subsequent corneometer and CRS imaging measurements were then performed 2 more times at 1-hour intervals. This investigation was performed using specimens from 3 different patients. Of note, the third timepoint data for Patient #3 could not be collected, as the epidermis of the skin sample on the gel substrate was compromised after the second timepoint. For this reason, only the data collected from the first two timepoints for Patient #3 was included in the statistical analysis.

2.6. Skin explant rehydration

To study the effects of moisturizing compounds on dry skin, four sets of skin samples were necessary per patient. All samples were first processed and maintained in an incubator as described above in order to attain a stable hydrated state. Next, all samples were removed from the incubator and allowed to dry in plastic dishes under ambient atmospheric conditions for 2 hours to allow the skin to dry and reach a stable dehydrated state, as confirmed by corneometry. The samples were then subjected to corneometry and CRS imaging before undergoing moisturizer treatment in order to assess the hydration status of the baseline dehydrated state, to be used as the reference for all rehydration comparisons. To this aim, two moisturizing compounds were used, namely 12% deuterated glycerin dissolved in water, and 0.25% hyaluronic acid dissolved in water, designed to match typical humectant concentrations found in commercial formulations [34, 35]. The deuterated form of glycerin was selected in order to avoid CRS signal generation from its CH_2 and OH moieties. This was not a concern in the case of hyaluronic acid for two reasons: (1) its concentration was nearly 50-fold lower, and (2) it does not contain any CH_2 groups. Thus, the only potential source of spectral cross-talk are the molecule's OH groups, but they are dwarfed in numbers by the surrounding water molecules. Of each treatment pair, one subset was returned to the incubator, while the other remained at ambient conditions. Additional CRS and corneometer measurements were obtained 2 more times at 1-hour intervals. As above, this investigation was also performed using specimens from 3 different patients. Of note, the samples treated with glycerin absorbed the formulation over the time course of the experiment, allowing for a straightforward assessment of the stratum corneum using corneometry and CRS imaging. The skin samples treated with hyaluronic acid, on the other hand, remained noticeably wet at their surface throughout the experimental time course, barring any assessment at the second timepoint without perturbing rehydration dynamics. For the final timepoint, the residual moisture on the skin surface was carefully wiped with delicate task wipers prior to data collection.

2.7. Statistical analysis

Processed image data was analyzed using the notebooks written in the R language. Data was analyzed using R 3.4.1 within the RStudio environment with extra packages compiled from the R 3.4.3 distribution. Correlation tests were first used to assess whether certain image analysis outcomes were independent since spectral overlap between the probed vibrational bands of interest was considered a potential factor between different chemical weightings (e.g. lipid vs. protein). To examine correlation, Pearson's R was calculated between image analysis outcomes in a pairwise manner with a coefficient of correlation greater than 0.9 considered to be highly correlated. Highly correlated outcomes were considered potentially linked due to spectral overlap.

Biomedical Optics EXPRESS

The outcomes calculated from image analysis such as cellular water content measured via SRS were each subjected to linear regression analysis for longitudinal data. Cell- and region-specific information was collected from 3 distinct imaging areas across multiple subjects. As these areas and subjects were statistically exchangeable, they were considered random factors in the analysis. Linear regression was performed through the use of linear mixed effect models using the *lme4* and *lmerTest* R packages. In the initial analysis, individual image analysis outcomes were tested serially via linear mixed effect model regression analysis where the timepoint was treated as a fixed factor. Subject was considered a random factor and tissue area considered a random factor nested within each subject. For each image analysis outcome, the effect size β, t-statistic, and p-value were calculated and tabulated. It should be noted that while a threshold of 0.05 is conventionally set for p-values in order to determine significance, linear regression was performed once for each imaging metric across all paired conditions. Thus, for the dehydration experiment, the Holm-Bonferroni correction was used to compensate for family-wise error.

To compare conditions and assess the effect of treatments, a linear mixed effect model regression equation was built using the categorical treatment condition values as independent indicator variables. The baseline comparator condition was set as ambient environment without topical treatment. The regression equation specifically included not only the timepoint of the outcome, but also a timepoint-condition interaction term to separately test whether the treatment condition was a modifier for the time-dependent outcome. As above, the Holm-Bonferroni method was used to compensate for family wise error.

3. Results and discussion

3.1. CRS imaging metrics

The focus of this study was to build an imaging and analysis method for the chemical and morphological characterization of the stratum corneum under changing hydration conditions. An *ex vivo* skin model was imaged with CRS microscopy techniques without *a priori* biases such that the data could be assessed post-acquisition using mathematical and statistical methods. As an exploratory characterization study, the number of subjects was initially set at $N = 3$ per experiment, noting that hundreds of individual cells and their associated parameters were measured to characterize changes in skin.

For non-invasive investigations of human skin in a laboratory setting, *ex vivo* human skin samples acquired from discarded tissues as a result of elective patient surgeries are typically used as a model to recapitulate the active physiology of a living individual's skin [36, 37]. In the context of this study, such human skin explants were imaged via CRS microscopy to visualize the architecture and biochemical content of the stratum corneum. Hydration-relevant parameters such as lipid content can be measured by probing the symmetric CH_2 stretching vibrational mode at 2845 cm^{-1} [25] while the CH_3 molecular vibration at 2950 cm^{-1} can be used to detect proteins by their hydrophobic amino acids with methyl groups [38]. Water molecules themselves can be readily detected by probing the strong OH stretching vibrational mode at 3220 cm^{-1} [39], characteristic of water molecules bound by hydrogen bonds.

Representative CARS and SRS images of the stratum corneum acquired simultaneously by probing each of the three vibrational bands of interest are shown in Fig. 1, illustrating the particularly strong contrast observed between the intracellular and extracellular spaces. Corneocytes appear as polygonal cells surrounded by a bright extracellular matrix rich in lipids (Fig. 1(a,d)) and proteins (Fig. 1(b,e)). Water content (Fig. 1(c,f)), on the other hand, is mostly confined within the corneocyte cell bodies, with a much lower abundance in the extracellular space.

While both imaging modalities generate similar contrast, CARS images uniquely contain an inherent background anti-Stokes signal that is generated independently of Raman-active molecules, known as the non-resonant background (NRB). While the anatomical features in

Biomedical Optics EXPRESS

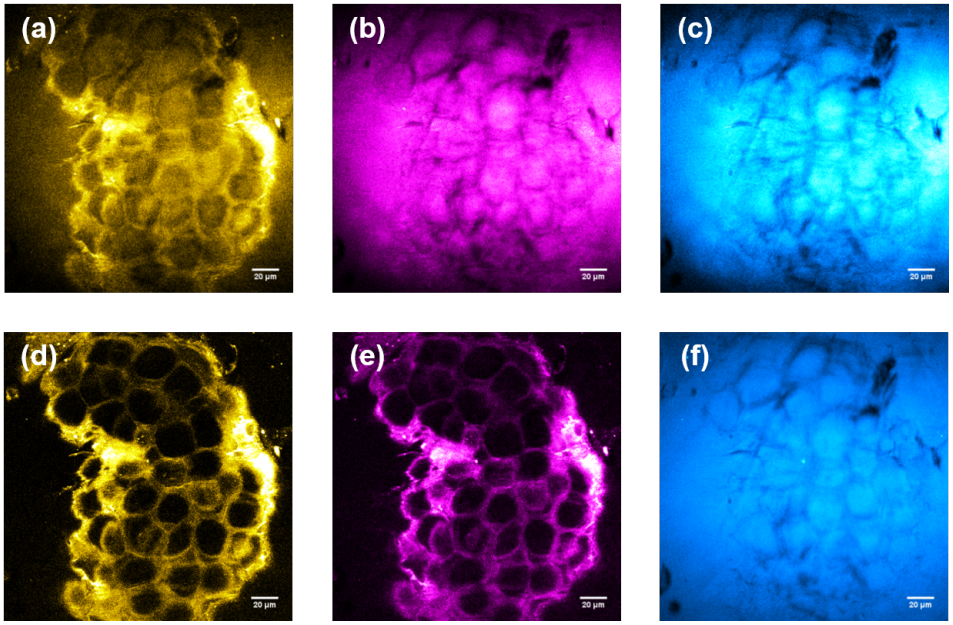

Fig. 1. CRS images of human stratum corneum acquired from *ex vivo* skin explants. (a–c) CARS and (d–f) SRS images of stratum corneum showing (a,d) lipid-weighted content; (b,e) protein-weighted content; and (c,f) water-weighted content. The NRB in the CARS data manifests itself as a homogeneous and unspecific haze distributed across the field of view.

CARS images of the stratum corneum can be readily appreciated, the interpretation of individual pixel values becomes challenging due to the unspecific contribution from the NRB, which manifests as a broad and homogenous distribution of background signal centered within the field of view. Importantly, the generation of NRB is exclusive to CARS; the SRS signals in Fig. 1(d–f) strictly arise from the targeted Raman-active molecules. Conveniently, since these processes occur simultaneously, the acquisition of CARS data in addition to SRS comes at no additional cost.

The CRS microscopy platform used to image human stratum corneum in the context of this study was capable of generated a total of 35 imaging metrics, although not all metrics were found to be of value, as will be discussed later. First, the system is equipped with two simultaneous imaging modalities (i.e. CARS and SRS) to probe the distribution of three chemical species of interest, namely lipids, proteins, and water, thereby generating 6 metrics. The relative ratios between these chemical species (i.e. lipid-to-protein, lipid-to-water, and protein-to-water) can also be assessed by computing image intensity ratios on a pixel-by-pixel basis, thus bringing the metric count to 12. With manual segmentation of corneocytes and generation of regions of interest (ROIs) as shown in Fig. 2, each of the 12 previously defined metrics can be redefined with respect to anatomical component (i.e. intracellular vs. extracellular). This then doubles the metric count once more for a total of 24 metrics regarding skin hydration. By further considering intracellular-to-extracellular ratios of chemical content for both modalities, 6 more metrics are added to the count. Finally, using the manually generated ROIs for each corneocyte, 5 morphological parameters can be defined based on cellular geometry: cell diameter, perimeter, and circularity, as well as the nearest neighbor distances (NND) between adjacent corneocyte cell centers ($NND_{Centers}$) and cell walls (NND_{Walls}). Together with corneometer measurements acquired in parallel with CRS imaging, this investigative toolkit is therefore capable of characterizing 36 observable morphological and chemical metrics for each skin sample at a given timepoint under a particular set of experimental

Biomedical Optics EXPRESS

conditions. However, imaging metrics generated using CARS microscopy were ultimately discarded due to the generation of strong NRB resulting in poorly interpretable longitudinal data.

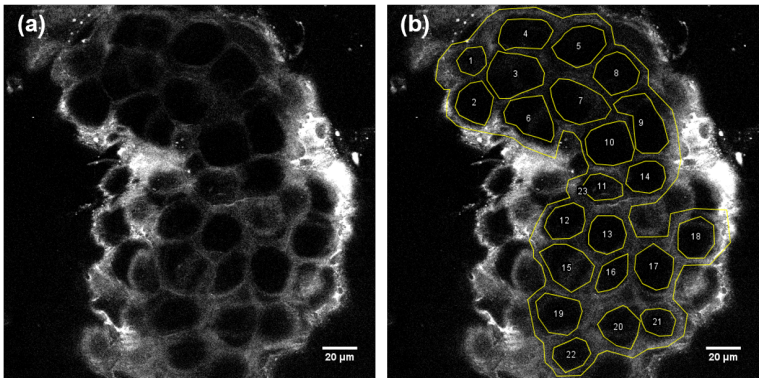

Fig. 2. Manual segmentation of SRS lipid content image to distinguish intracellular and extracellular spaces for subsequent analysis. (a) Unlabeled image. (b) Manually segmented image, showing corneocytes identified by indices 1 through 22, and extracellular space corresponding to the surrounding region identified by index number 23.

Initial assessment of the acquired CRS imaging data found a strikingly similar contrast in the protein and lipid channels across all experimental conditions (Fig. 1(d,e), for example). This is not surprising, as femtosecond laser sources such as the one used in this study have an inherently broad frequency spectrum. As such, such laser sources can generate strong CRS signals at the cost of decreased spectral specificity [25]. Following acquisition of the imaging data, it was unclear whether the observed similarities truly illustrated correlations in the distribution of lipids and proteins, or whether the femtosecond laser sources used were too spectrally broad to resolve the two vibrational peaks of interest (2845 and 2950 cm^{-1} for lipids and proteins, respectively). To verify whether this was indeed the case, the SRS lipid and protein chemical content image sets were statistically analyzed to determine whether the observed SRS lipid intensity in each cell could be explained by its corresponding SRS protein intensity. A strong correlation was indeed observed between the SRS lipid and protein signals (Pearson's $R = 0.921$). This lipid-protein correlation was less strong in the case of CARS, but nevertheless significant (Pearson's $R = 0.812$). Therefore, protein-associated imaging metrics were not considered for the statistical analysis of the dehydration and rehydration results that follow. It is worth noting, however, that methods to increase the spectral specificity in femtosecond CRS microscopy — collectively referred to as "spectral focusing" — have been previously reported [38,40,41], and can be implemented to include the ability to reliably probe protein content within cells and tissues.

3.2. Stratum corneum dehydration

For the dehydration investigation, *ex vivo* skin explants were first imaged with CRS microscopy and probed with the corneometer immediately upon retrieval from the incubator. Following the first set of data acquisition, one set of skin samples was allowed to dry on a plastic substrate while the other was maintained in parallel on its nutritive gel under ambient conditions bed to limit dehydration. Imaging was then performed at two additional timepoints alongside corneometer measurements performed in triplicates for each experimental timepoint and each treatment condition. The corneometer data is shown over time for both the dehydrated and moist conditions in Fig. 3, and illustrates a net overall decrease in skin hydration as the skin samples are left to dry. As expected, the skin samples that were maintained on the moist gel bed retained their hydration

Biomedical Optics EXPRESS

more efficiently.

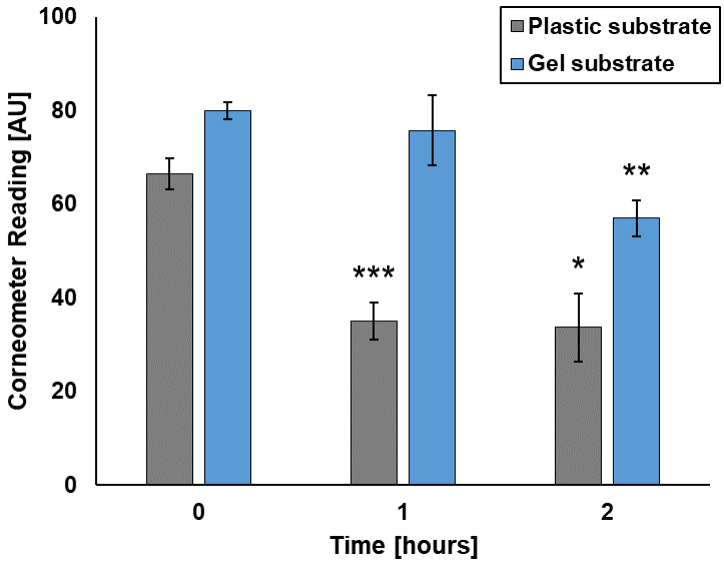

Fig. 3. Corneometer measurements obtained from *ex vivo* human skin throughout the dehydration time course on a plastic substrate (i.e. rapid dehydration) and a gel substrate (i.e. slow dehydration). Data points correspond to the mean of the triplicate corneometer measurements with error bars indicating the standard error of the mean. Statistically significant deviations from the corresponding initial timepoint are denoted by asterisks and determined via Student's t-test (*: $p < 0.05/N$; **: $p < 0.01/N$; ***: $p < 0.001/N$, adjusted using Bonferroni correction with $N = 4$ pairwise comparisons).

Linear regression analysis was performed for each CRS imaging metric and corneometer measurement in order to find statistically significant trends over time and to investigate the environmental influence on these dynamics. A linear mixed effect model for each metric was designed to explore the possibility of modeling each observed metric as a linear function of time (a fixed factor). Each patient was considered as a random factor and each field of view per patient as a nested random factor within each patient, given that each skin sample for each patient was imaged at 3 different areas per treatment condition. Note that the given area imaged at each timepoint was different. As opposed to a marginal model which would indiscriminately consider the means from all subjects together, this conditional model approach allows for subject-specific statistical analysis. Given that patient number and patient sample area were exchangeable (since all samples were completely anonymized), they could readily be assigned as random factors. The linear mixed model was adopted while holding the treatment condition constant by first modeling the data collected under the rapid drying condition before modeling the kinetics of slowed dehydration over a moist nutritive gel substrate.

CARS imaging data was closely explored during this step of the analysis. As mentioned above, CARS microscopy images contain both a chemically specific response as well as a nonspecific response (i.e. NRB). This latter nonspecific response arises as a function of the density of a given material and its electronic polarizability; these two factors mix to give rise to a coherent signal that adds to the chemically specific signal. In analyzing the CARS imaging data, it became clear that the CARS data contained at least two responses to dehydration: not only were there changes in the chemical content of the skin, but there were changes in cellular morphology as well. These morphological changes, which included changes in tissue thickness, cell size, and

Biomedical Optics EXPRESS

intercellular distance, could lead to variations in the proportion of the CARS signal that arises from non-resonant contributions. As this nonspecific factor leads to chemically independent changes in the total CARS signal intensity [25], chemically-weighted CARS imaging data was not included in the statistical analysis. CARS imaging is therefore used to inform manual image segmentation and morphological assessment, i.e. metrics independent of chemical signatures.

The hourly rates of change for each metric under both dehydration conditions are listed in Table 1 along with the 95% confidence intervals and *p*-values. The most significant changes observed under both conditions were primarily morphological, with parameters such as cell diameter and perimeter seen to decrease, while the NND between cell walls was observed to increase. These observations suggest that corneocytes undergo a generalized decrease in size as they dehydrate in addition to progressively retracting away from one another, consistent with previous findings using cryo-scanning electron microscopy [23].

As seen in Table 1, relative water content as determined by SRS water intensity was found to decrease at an average rate of approximately 7% per hour for both intracellular and extracellular spaces under the dry environmental condition. This rapid dehydration rate was diminished by the wet gel substrate where the time-dependent variation of tissue water content was no longer significant. Interestingly, these changes are also reflected in the corneometry measurements where a dramatic dehydration rate of -15.3 units per hour was recorded on the plastic substrate while the corresponding rate on the gel substrate was found to be roughly 35% slower (i.e. -9.92 units per hour). The lipid-to-water ratio in both intracellular and extracellular spaces was consistently seen to increase only under the dry condition and more so in the case of the extracellular space. While the intracellular lipid content also decreased slightly over time under both conditions, this decrease was more rapid over the plastic substrate which further contributed to the contrast in lipid-to-water ratios between the two experimental conditions. While the decrease in water content can simply be attributed to tissue dehydration, the change in lipid content is more nuanced. It is possible that during the dehydration process, some of the stratum corneum lipids are rearranged into deeper skin layers; this could occur as the drying stratum corneum becomes stiff, forcing motile lipids beneath. It further cannot be excluded that sample handling may have further impacted the overall composition of the extracellular lipid matrix once it had already begun to deteriorate. Given that each timepoint involved interrogation of the tissue sample using both the corneometer and the microscope (both modalities involving direct contact with the skin surface), it is therefore possible that a small portion of the lipids from the skin surface were lost to the corneometer probe or the glass-bottom dishes used for imaging.

Despite the small number of patient samples, this imaging based approach was able to measure and visualize a large number of cells needed to generate a significant body of data. Overall, marked differences in hydration dynamics were observed between *ex vivo* patient samples depending on the type of substrate, most strikingly in the case of intracellular water content assessed via SRS microscopy. Given these newfound nuances, the proposed methodology supports the applicability of using CRS imaging to complement corneometry in order to non-invasively and non-destructively measure cellular morphology and probe hydration-relevant metrics with subcellular resolution. Whereas corneometry relies on making bulk 1 cm^2 point measurements that extends down to the dermal layer, CRS imaging in the context of this study was able to detect subtle chemical changes in a micron-thin slice of the stratum corneum on a pixel-by-pixel basis. With a field of view of 212×212 μm^2, objects such as single corneocytes and entire extracellular spaces surrounding collections of corneocytes can be analyzed at high resolution with chemical specificity. Thus, while total probed volume for CRS measurements is several orders of magnitude smaller than that of the corneometer, it can still serve as a useful complementary tool between in hydration studies.

Biomedical Optics EXPRESS

Table 1. Stratum corneum metric dynamics measured over the time course of *ex vivo* human skin dehydration on two different substrates. For the plastic substrate, asterisks denote rates of change significantly different from zero; for the gel substrate, they denote rates of change that are significantly different from the plastic substrate (*: $p < 0.05$; **: $p < 0.01$; ***: $p < 0.001$, where p-values are adjusted using Holm-Bonferroni correction with $N = 36$ metrics. IER: intracellular-to-extracellular ratio; NND: nearest neighbor distance; CI: confidence interval.)

METRIC	PLASTIC SUBSTRATE			GEL SUBSTRATE		
	Hourly rate of change	95% CI	p-value	Hourly rate of change	95% CI	p-value
Corneometry						
Corneometer	-15.3 **	[-22.1, -8.57]	3.13×10^{-3}	-9.92	[-21.6, 1.79]	1.00
Water content						
Intracellular	-6.66 % ***	[-8.35, -4.97] %	1.38×10^{-5}	-2.46 % ***	[-4.33, -0.60] %	2.90×10^{-22}
Extracellular	-6.95 % ***	[-9.08, -4.82] %	1.26×10^{-5}	-1.98 %	[-5.67, 1.71] %	6.84×10^{-2}
IER	0.17 %	[-0.18, 0.53] %	1.00	-0.42 %	[-1.03, 0.19] %	0.543
Lipid content						
Intracellular	-4.42 %	[-6.62, -2.21] %	7.55×10^{-2}	-2.56 % ***	[-4.86, -0.27] %	1.43×10^{-6}
Extracellular	-3.20 %	[-5.96, -0.44] %	1.00	-2.74 %	[-6.41, 0.92] %	1.00
IER	-1.23 %	[-2.57, 0.11] %	0.821	0.14 %	[-2.02, 2.29] %	1.00
Lipid-to-water ratio						
Intracellular	2.26 %	[0.61, 3.91] %	0.256	-0.02 % ***	[-1.85, 1.81] %	5.74×10^{-7}
Extracellular	3.73 % *	[1.88, 5.57] %	1.48×10^{-2}	-0.49 % *	[-3.14, 2.17] %	1.44×10^{-2}
Morphology						
Cell diameter	-7.06 μm *	[-14.6, 0.51] μm	4.94×10^{-2}	-3.97 μm	[-13.0, 5.09] μm	0.545
Cell perimeter	-4.92 μm	[-8.70, -1.13] μm	0.756	-3.61 μm	[-9.58, 2.36] μm	1.00
$NND_{Centers}$	-0.28 μm	[-0.96, 0.41] μm	1.00	0.45 μm	[-0.54, 1.45] μm	0.912
NND_{Walls}	2.01 μm	[0.79, 3.23] μm	0.0265	1.11 μm	[-0.75, 2.97] μm	1.00

3.3. Stratum corneum rehydration

The second portion of this study was focused on the rehydration dynamics of skin following topical application of two humectant agents: glycerin and hyaluronic acid. To simulate dehydrated skin tissue, *ex vivo* skin explants were removed from the incubator and allowed to dry under ambient conditions prior to humectant treatment. As confirmed by a plateau in the corneometer hydration measurements, samples in this model approach were considered dehydrated at the initial timepoint of the CRS rehydration study. Experiments were carried out in subject batches, where each batch encompassed a single day of experiments of all conditions on all tissue samples from a single subject.

Linear mixed effect model regression analysis was performed for each CRS imaging metric along with corneometer measurements in order to find statistically significant trends in treatment response over time and to investigate the environmental influence on these dynamics. While glycerin and hyaluronic acid have distinct dermal penetration kinetics [7], their use in topical formulations is intended to impart a therapeutic effect within the minutes and hours following application. Their longitudinal effects on the stratum corneum can thus be accurately captured over a two-hour rehydration time course.

Corneometer measurements performed throughout the various rehydration condition time courses are shown in Fig. 4. From the results, it can be seen that the sample left under ambient conditions without topical treatment continued to dehydrate slightly, albeit without statistical significance. Interestingly, all treatment conditions significantly improved the rehydration rate and successfully restored skin hydration as verified by corneometry.

Interestingly, the most significant metric impacted by both time course and topical treatment was the intracellular water and lipid contents of corneocytes as measured by SRS microscopy

Biomedical Optics EXPRESS

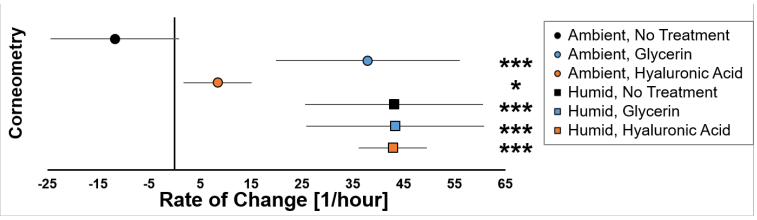

Fig. 4. Corneometry-based assessment of *ex vivo* human skin hydration dynamics during rehydration under various environmental and treatment conditions. Data points correspond to the rate of change of corneometer measurements per hour, with error bars showing the 95% confidence interval. For the ambient condition without treatment (control), asterisks denote rates of change significantly different from zero; for all other conditions, they denote rates of change that are significantly different from the control (*: $p < 0.05$; **: $p < 0.01$; ***: $p < 0.001$, where p-values are adjusted using Holm-Bonferroni correction with $N = 36$ metrics).

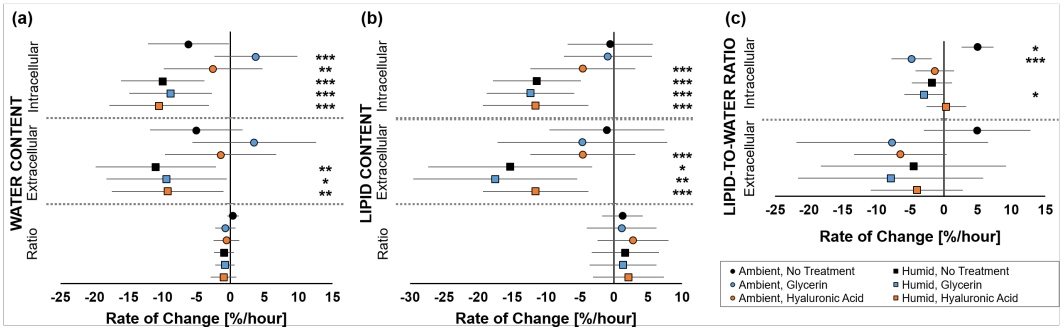

Fig. 5. Chemical content dynamics of *ex vivo* human skin during rehydration under various environmental and treatment conditions. Data points correspond to the rate of change of CRS imaging metrics per hour, with error bars showing the 95% confidence interval. For the ambient condition without treatment (control), asterisks denote rates of change significantly different from zero; for all other conditions, they denote rates of change that are significantly different from the control (*: $p < 0.05$; **: $p < 0.01$; ***: $p < 0.001$, where p-values are adjusted using Holm-Bonferroni correction with $N = 36$ metrics).

(Fig. 5(a,b)). Under both dry and hydrated conditions, the intracellular water and lipid contents were found to decrease over time, except in the event of glycerin application under ambient conditions — the only condition where intracellular chemical content increased at a positive rate. This was also the condition under which the intracellular lipid-to-water ratio decreased most significantly throughout the rehydration process (Fig. 5(c)). In contrast to these CRS results, corneometry indicated an increase in skin hydration following both glycerin and hyaluronic acid treatment, although the hydration increase following the latter treatment was less pronounced under ambient environmental conditions. These findings suggest the possibility that, in this *ex vivo* model system, the water retained by the tissue following humectant application is taken up but not necessarily retained in corneocyte cell bodies. This disagreement is not necessarily problematic: while corneometry is considered most sensitive to the topmost 15 to 45 μm of the interrogated sample, its bulk probing volume actually extends several tens of microns deeper into the skin albeit with decreasing sensitivity [17, 42]. This lack of spatial specificity may result in a significant portion of the viable epidermis and dermis being interrogated as well, which could explain the apparent discrepancy in the changes in corneocyte water content as measured by SRS

Biomedical Optics EXPRESS

imaging.

Of note, the diameter of cells treated with glycerin was also observed to gradually increase over the time course of the experiment under all conditions with the exception of glycerin treatment in the humid incubator environment. This observation may be interpreted as a transient swelling of the cells over time, however, without statistically significant retention of hydration (Fig. 6). This correlation between corneocyte size and hydration is generally consistent with previous findings assessed via cryo-scanning electron microscopy [23].

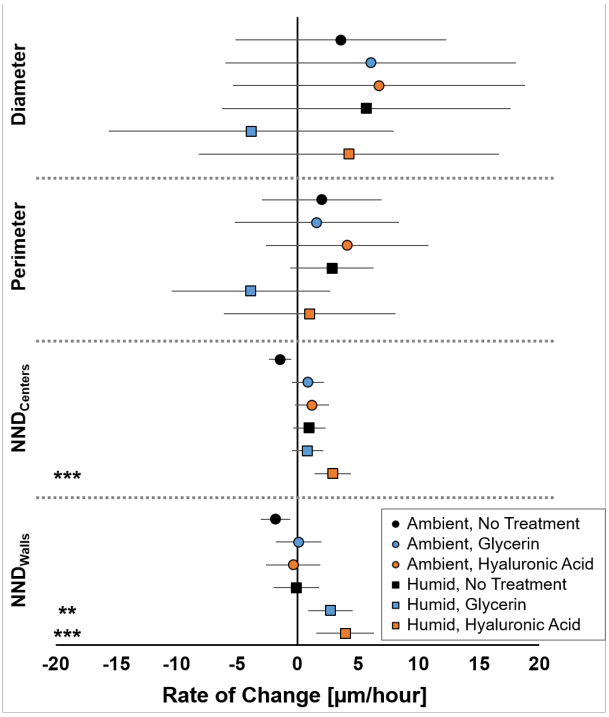

Fig. 6. Morphological dynamics of *ex vivo* human corneocytes during rehydration under various environmental and treatment conditions. Data points correspond to the rate of change of each spatial metric in microns per hour with error bars showing the 95% confidence interval. Nearest neighbor distances are computed between corneocyte cell centers ($NND_{Centers}$) as well as between cell walls (NND_{Walls}). For the ambient condition without treatment (control), asterisks denote rates of change significantly different from zero; for all other conditions, they denote rates of change that are significantly different from the control (*: $p < 0.05$; **: $p < 0.01$; ***: $p < 0.001$, where p-values are adjusted using Holm-Bonferroni correction with $N = 36$ metrics).

Skin explants treated with hyaluronic acid and left to rehydrate under ambient conditions showed an overall decrease in terms of intracellular water content, although these changes differed in magnitude from their untreated counterparts in a statistically significant manner. Indeed, under ambient conditions, the intracellular water loss was slowed, while the humid and warm environment of the incubator was found to exacerbate the water loss rate. This overall trend is consistent with that observed in samples treated with glycerin. Interestingly, the intracellular lipid content in the hyaluronic acid treated explants under ambient conditions was now found to decrease at a significantly accelerated rate relative to the untreated samples. It is also worth noting that some aspects of cellular morphology were also impacted by hyaluronic acid treatment under ambient conditions. In particular, the hyaluronic acid treatment under the humid and warm

Biomedical Optics EXPRESS

conditions of the tissue incubator resulted in increased distances between corneocyte cell centers and their walls, suggestive of tissue swelling as a result of increased hydration.

It is also worth examining the overall similarities and differences in the samples kept at room temperature relative to those maintained in the tissue incubator at 37°C, 5% atmospheric CO_2, and 95% relative humidity between measurements. The warm and humid environment of the incubator was found to significantly affect the water and lipid loss rates, with intracellular loss rates increasing 2- and 3-fold, respectively, relative to the untreated sample under ambient conditions. The extracellular water and lipid contents were also found to decrease significantly, which was otherwise only observed in the case of hyaluronic acid treatment under ambient conditions. Despite this radical shift in water content throughout the stratum corneum, the corneometer nevertheless measured a dramatic rise in skin hydration, similar in magnitude to a topical application of glycerin under ambient conditions. This discrepancy highlights the difference in probing volumes between corneometry and water content assessment via SRS microscopy.

When skin samples were treated with either glycerin or hyaluronic acid and maintained in the incubator between measurements, the observed trends generally resembled those of untreated incubated skin: the intracellular and extracellular water and lipid loss rates increased significantly, despite corneometry showing a marked increase in terms of skin hydration. Corneocyte morphology, however, was generally found to remain unaffected, other than in the particular case of hyaluronic acid treatment under humid and warm conditions as noted above.

Table 2. Summary of observed changes over the time course of skin explant rehydration. (N/C: no change; +++, ++, +: strong, moderate, and modest increase, respectively; – – –, – –, –: strong, moderate, and modest decrease, respectively.)

METRIC	AMBIENT ENVIRONMENT			HUMID ENVIRONMENT		
	No treatment	Glycerin	Hyaluronic acid	No treatment	Glycerin	Hyaluronic acid
Corneometry						
Corneometer	–	+++	+	+++	+++	+++
Water content						
Intracellular	– –	+	–	– – –	– – –	– – –
Extracellular	N/C	N/C	N/C	– – –	– – –	– – –
IER	N/C	N/C	N/C	N/C	N/C	N/C
Lipid content						
Intracellular	N/C	N/C	–	– – –	– – –	– – –
Extracellular	N/C	N/C	–	– – –	– – –	– – –
IER	N/C	N/C	N/C	N/C	N/C	N/C
Lipid-to-water ratio						
Intracellular	+	– –	N/C	N/C	–	N/C
Extracellular	N/C	N/C	N/C	N/C	N/C	N/C
Morphology						
Cell diameter	N/C	N/C	N/C	N/C	N/C	N/C
Cell perimeter	N/C	N/C	N/C	N/C	N/C	N/C
$NND_{Centers}$	N/C	N/C	N/C	N/C	N/C	+
NND_{Walls}	N/C	N/C	N/C	N/C	+	++

A summary of all observable metrics that show variability over time is presented in Table 2. As demonstrated by corneometry, skin samples required the warm and humid environment of the incubator and/or a topical application of glycerin or hyaluronic acid in order to rehydrate. The SRS imaging results point to an interesting suggestion that the stratum corneum itself may not retain or increase its water content within corneocytes during glycerin and hyaluronic acid induced rehydration. In fact, in this *ex vivo* model system, the SRS imaging results indicate that the rate of intracellular water loss from the stratum corneum accelerated for all conditions

Biomedical Optics EXPRESS

under the warm and humid incubator conditions. It should be noted that calculations carried out on the CARS images (data not shown) show the opposite overall trend, an effect that is hypothesized to arise from two factors. First, as noted above, structural changes to the skin are likely to cause changes to the non-resonant signal contribution that contaminates the CARS signal. Second, an additional non-resonant contribution in the CARS images arises from the glycerin and hyaluronic acid treatments themselves, creating a false increase in apparent water content. The SRS imaging data, which instead scales linearly with molecular concentration and does not contain non-resonant signal contributions, clearly points to a net dehydration effect in all tested model samples.

Interestingly, this finding does not exactly agree with conventional understanding of stratum corneum behavior, warranting further discussion. First, it should be kept in mind that while the data is generated from many dozens of cells over many tissue samples, all samples were derived from a small set of subjects who underwent surgery. Discarded *ex vivo* tissue samples from these procedures were transported under cold, wet conditions prior to processing and placement into the tissue explant culture system for one to three days. It is therefore important to note that this *ex vivo* skin explant model may not be entirely representative of normal, healthy skin. Despite this fact, skin explant models are used widely in biological, cosmetic, and drug studies [36, 37, 43], highlighting the importance of understanding how they respond to various challenges and conditions on the cellular level.

Second, the dehydration approach used in this study approximated, but did not match, normal skin drying in humans. Dry skin *in vivo* involves changes and alterations in skin cellular biology that can occur over the course of days and weeks. The drying method used here created a bulk dehydration of thinned skin samples in mere hours, and may have driven the skin to states not normally experienced *in vivo*. While this caveat may not apply to skin undergoing the initial stages of dehydration, it may indeed affect rehydration. In addition, the mechanism responsible for tissue rehydration may differ here from a more realistic *in vivo* scenario. In cases where the skin's barrier function is disrupted, some topical agents are designed to form an artificial barrier at the skin surface, thereby allowing the epidermal layers of skin to rehydrate via diffusion of internal hydration as opposed to recruiting atmospheric water. This mechanism would be interesting to study with *in vivo* coherent Raman imaging tools. In the case of this experiment, as the dehydration/rehydration approach is used in research [43, 44], it is important to understand the implications of findings derived from such models.

It is furthermore worth recalling that CRS imaging modalities are non-destructive techniques that assesses chemical content directly based on the intrinsic molecular vibrations of the chemical groups of interest. Other techniques have previously been used to study stratum corneum hydration including high pressure freezing before freeze substitution [45] and cryo-scanning electron microscopy [23], although in using such investigational approaches, it cannot be excluded that the harsh tissue processing protocols affect the integrity of the corneocytes themselves. CRS microscopy methods therefore offer the advantage of requiring little-to-no sample preparation, and have already been used to pursue dermatological investigations in human subjects [46]. Having an established framework for processing CRS image data using linear mixed effect models, investigations can further be performed on human volunteers in order to ascertain stratum corneum hydration dynamics in the most ideal biological context *in vivo*.

The discrepancy in hydration between corneometry and CRS imaging in the present model system is thought to arise from both the volumes of tissue interrogates and the nature of the measurement itself. Nonlinear optical imaging techniques such as SRS are able to probe focal volumes on the scale of the cubic micron with three-dimensional spatial resolution. In contrast, the current industry standard for hydration measurements, corneometry, is known to integrate signals over several tens of microns and can encompass all layers of the epidermis beyond the stratum corneum as well as a portion of the dermis within human skin. Whereas CRS imaging

Biomedical Optics EXPRESS

directly measures the concentration of given molecular species such as water, corneometry indirectly measures tissue water content via quantification of capacitance. This difference highlights the need for complementary chemically sensitive CRS microscopy techniques with corneometry. The CRS imaging method developed for this study does indeed suggest something unexpected occurring to the stratum corneum, a finding that is not anticipated by the corneometry measurements alone. The *ex vivo* models in this study experienced major, opposite changes in water content between bulk tissue and the stratum corneum under conditions that were expected to lead to tissue rehydration.

4. Conclusion

The results in the present work strongly suggest the need for future studies that make use of improved model systems, increased subject numbers, and perhaps a pivot to *in vivo* experiments. For the reasons discussed above, improved tissue sources and model systems should be explored. Optimized and traceable skin explant cultures can now be purchased from commercial vendors such as Genoskin Inc., providing improved tissue cultures that remain viable for substantially longer time courses than models such as those used in the present study. Genoskin and similar vendors can also provide tissues from a wider range of donors, which can increase subject numbers to ensure that results arise from respective populations. Ultimately, however, these experiments should transition away from model systems to *in vivo* studies. Skin culture models are only a way to prolong the eventual decay of *ex vivo* skin tissue, and dehydration/rehydration models can never fully match real dry skin.

To meet these clinical research needs, we are developing new, portable CARS and SRS microscopy systems with the goal of carrying out *in vivo* CRS imaging of skin in the near future. A portable clinic-ready imaging system will be key to visualize dry or compromised skin and capture the full biological dynamics of treatment response. Such an instrument can also incorporate additional detection methods and imaging modalities, including two-photon excited fluorescence (TPEF), which can be used to probe coenzymes such as flavin and nicotinamide adenine dinucleotides (FAD and NADH, respectively) to probe metabolic perturbations [26, 37]; transient and sum-frequency absorption (TA and SFA, respectively) to probe the strong absorptive properties of pigments and chromophores such as melanin species and hemoglobin [47–49]; as well as second harmonic generation (SHG), which relies on the birefringent nature of collagen fibers to generate a strong signal that maps oriented extracellular matrix proteins without the use of exogenous labels [50]. These imaging techniques can be judiciously combined with one another to best complement standard measurement techniques to tease out the detailed biological response to dehydration and rehydration.

In the present study, investigations were limited to the stratum corneum, where each imaging field of view typically contained a few tens of corneocytes that, together with the extracellular space, translated to tens of observations. In exploring other layers of skin with additional nonlinear imaging techniques such as those described above, this methodological approach to assessing imaging metrics therefore allows one to easily record many hundreds or even thousands of observables, each defined by a handful of categorical descriptors such as patient number or treatment condition. Programming languages such as Matlab and Python lend themselves particularly well to processing such datasets, as the computations involve iterative processing of multichannel image data with binary masks generated via manual segmentation. The image analysis then returns a data table where each row corresponds to an individual observation, and each vector corresponds to either a descriptor (e.g. patient number, treatment condition, timepoint, etc.) or an observed metric (e.g. water content, lipid content, cell diameter, etc.). Such data formats are ideal for statistical software packages such as R, where linear mixed effect models can serve to identify longitudinal trends and differences between treatment conditions.

Further work in assessing chemical content across the various strata of human skin using CRS

Biomedical Optics EXPRESS

microscopy (and other complementary nonlinear optical imaging methods) may also further inform the development of new topical formulations; combining these imaging toolkits with corneometry will further shed light on both the microscopic and macroscopic effects of topical treatment strategies.

Funding

This study was funded via a sponsored research agreement between Massachusetts General Hospital and The Estée Lauder Companies, Inc. This work was also conducted with support from Harvard Catalyst | The Harvard Clinical and Translational Science Center (National Center for Advancing Translational Sciences, National Institutes of Health Award UL 1TR002541) and financial contributions from Harvard University and its affiliated academic healthcare centers. The content is solely the responsibility of the authors and does not necessarily represent the official views of Harvard Catalyst, Harvard University and its affiliated academic healthcare centers, or the National Institutes of Health.

Acknowledgments

The authors would like to acknowledge the members of the Evans Group who have kindly agreed to aid in performing manual segmentation of acquired image sets, and for providing constructive feedback regarding the manuscript. The authors also acknowledge the help of Dr. Samuel Lin, Dr. Parisa Kamali, and Dr. Alexandra Bucknor for their assistance in obtaining tissue samples. Finally, the authors also acknowledge the many helpful discussions with Dr. Ying Kuen K. Cheung who provided valuable supplementary guidance on the statistical analysis performed herein.

Disclosures

JDC: The Estée Lauder Companies, Inc. (E), CF: The Estée Lauder Companies, Inc. (E), CLE: Massachusetts General Hospital (P,R). All other authors declare that there are no other conflicts of interest related to this article.

References

1. A. A. Romanovsky, "Skin temperature: its role in thermoregulation," Acta Physiol. **210**, 498–507 (2014).
2. Y. Belkaid and J. A. Segre, "Dialogue between skin microbiota and immunity," Science **346**, 954–959 (2014).
3. A. Zimmerman, L. Bai, and D. D. Ginty, "The gentle touch receptors of mammalian skin," Science **346**, 950–954 (2014).
4. D. D. Bikle, "Vitamin d metabolism and function in the skin," Mol. Cell. Endocrinol. **347**, 80–89 (2011).
5. E. Proksch, J. M. Brandner, and J.-M. Jensen, "The skin: an indispensable barrier," Exp. Dermatol. **17**, 1063–1072 (2008).
6. A. V. Rawlings and C. R. Harding, "Moisturization and skin barrier function," Dermatol. Ther. **17**, 43–48 (2004).
7. S. Verdier-Sévrain and F. Bonté, "Skin hydration: a review on its molecular mechanisms," J. Cosmet. Dermatol. **6**, 75–82 (2007).
8. A. Ishida-Yamamoto, S. Igawa, and M. Kishibe, "Order and disorder in corneocyte adhesion," The J. Dermatol. **38**, 645–654 (2011).
9. C. R. Harding, A. Watkinson, A. V. Rawlings, and I. R. Scott, "Dry skin, moisturization and corneodesmolysis," Int. J. Cosmet. Sci. **22**, 21–52 (2000).
10. A. V. Rawlings and P. J. Matts, "Stratum corneum moisturization at the molecular level: An update in relation to the dry skin cycle," J. Investig. Dermatol. **124**, 1099–1110 (2005).
11. M. Lodén, "Role of topical emollients and moisturizers in the treatment of dry skin barrier disorders," Am. J. Clin. Dermatol. **4**, 771–788 (2003).
12. A. V. Rawlings, "Trends in stratum corneum research and the management of dry skin conditions," Int. J. Cosmet. Sci. **25**, 63–95 (2003).
13. M. Lodén, "Effect of moisturizers on epidermal barrier function," Clin. Dermatol. **30**, 286–296 (2012).
14. C. L. Froebe, F. A. Simion, H. Ohlmeyer, L. D. Rhein, J. Mattai, R. H. Cagan, and S. E. Friberg, "Prevention of stratum corneum lipid phase transitions in vitro by glycerol — an alternative mechanism for skin moisturization," J. Soc. Cosmet. Chem. **41**, 51–65 (1990).

Biomedical Optics EXPRESS

15. U. Heinrich, U. Koop, M.-C. Leneveu-Duchemin, K. Osterrieder, S. Bielfeldt, C. Chkarnat, J. Degwert, D. Häntschel, S. Jaspers, H.-P. Nissen, M. Rohr, G. Schneider, and H. Tronnier, "Multicentre comparison of skin hydration in terms of physical-, physiological-and product-dependent parameters by the capacitive method (corneometer cm 825)," Int. J. Cosmet. Sci. **25**, 45–53 (2003).
16. P. Clarys, R. Clijsen, and A. O. Barel, "Influence of probe application pressure on in vitro and in vivo capacitance (corneometer cm 825®) and conductance (skicon 200 ex®) measurements," Ski. Res. Technol. **17**, 445–450 (2011).
17. P. Clarys, R. Clijsen, J. Taeymans, and A. O. Barel, "Hydration measurements of the stratum corneum: comparison between the capacitance method (digital version of the corneometer cm 825®) and the impedance method (skicon-200ex®)," Ski. Res. Technol. **18**, 316–323 (2012).
18. E. Alanen, J. Nuutinen, K. Nicklén, T. Lahtinen, and J. Mönkkönen, "Measurement of hydration in the stratum corneum with the moisturemeter and comparison with the corneometer," Ski. Res. Technol. **10**, 32–37 (2004).
19. J. W. Fluhr, R. Darlenski, N. Lachmann, C. Baudouin, P. Msika, C. De Belilovsky, and J.-P. Hachem, "Infant epidermal skin physiology: adaptation after birth," Br. J. Dermatol. **166**, 483–490 (2012).
20. W. J. Lee, J. Y. Kim, C. H. Song, H. D. Jung, S. H. Lee, S.-J. Lee, and D. W. Kim, "Disruption of barrier function in dermatophytosis and pityriasis versicolor," The J. Dermatol. **38**, 1049–1053 (2011).
21. A. E. Sagiv, S. Dikstein, and A. Ingber, "The efficiency of humectants as skin moisturizers in the presence of oil," Ski. Res. Technol. **7**, 32–35 (2001).
22. J. L. Sugarman, J. W. Fluhr, A. J. Fowler, T. Bruckner, T. L. Diepgen, and M. L. Williams, "The objective severity assessment of atopic dermatitis score: An objective measure using permeability barrier function and stratum corneum hydration with computer-assisted estimates for extent of disease," Arch. Dermatol. **139**, 1417–1422 (2003).
23. J. A. Bouwstra, A. de Graaff, G. S. Gooris, J. Nijsse, J. W. Wiechers, and A. C. van Aelst, "Water distribution and related morphology in human stratum corneum at different hydration levels," J. Investig. Dermatol. **120**, 750–758 (2003).
24. V. Andresen, S. Alexander, W.-M. Heupel, M. Hirschberg, R. M. Hoffman, and P. Friedl, "Infrared multiphoton microscopy: subcellular-resolved deep tissue imaging," Curr. Opin. Biotechnol. **20**, 54–62 (2009).
25. C. L. Evans and X. S. Xie, "Coherent anti-stokes raman scattering microscopy: Chemical imaging for biology and medicine," Annu. Rev. Anal. Chem. **1**, 883–909 (2008).
26. I. Georgakoudi and K. P. Quinn, "Optical imaging using endogenous contrast to assess metabolic state," Annu. Rev. Biomed. Eng. **14**, 351–367 (2012).
27. K. M. Hanson and C. J. Bardeen, "Application of nonlinear optical microscopy for imaging skin," Photochem. Photobiol. **85**, 33–44 (2009).
28. K. Koenig, "Hybrid multiphoton multimodal tomography of in vivo human skin," IntraVital **1**, 11–26 (2012).
29. H. Schneckenburger, P. Weber, M. Wagner, T. Bruns, V. Richter, S. Schickinger, and R. Wittig, "Multidimensional fluorescence microscopy in live cell imaging — a mini review," Photonics & Lasers Medicine **1**, 35–40 (2012).
30. C. Xu, W. Zipfel, J. B. Shear, R. M. Williams, and W. W. Webb, "Multiphoton fluorescence excitation: new spectral windows for biological nonlinear microscopy," Proc. Natl. Acad. Sci. **93**, 10763–10768 (1996).
31. L. A. Austin, S. Osseiran, and C. L. Evans, "Raman technologies in cancer diagnostics," Analyst **141**, 476–503 (2016).
32. C. H. Camp Jr and M. T. Cicerone, "Chemically sensitive bioimaging with coherent raman scattering," Nat. Photonics **9**, 295–305 (2015).
33. D. Zhang, P. Wang, M. N. Slipchenko, and J.-X. Cheng, "Fast vibrational imaging of single cells and tissues by stimulated raman scattering microscopy," Accounts Chem. Res. **47**, 2282–2290 (2014).
34. J. W. Fluhr, R. Darlenski, and C. Surber, "Glycerol and the skin: holistic approach to its origin and functions," Br. J. Dermatol. **159**, 23–34 (2008).
35. V. Liguori, C. Guillemin, G. F. Pesce, R. O. Mirimanoff, and J. Bernier, "Double-blind, randomized clinical study comparing hyaluronic acid cream to placebo in patients treated with radiotherapy," Radiother. Oncol. **42**, 155–161 (1997).
36. N. Mujahid, Y. Liang, R. Murakami, H. G. Choi, A. S. Dobry, J. Wang, Y. Suita, Q. Y. Weng, J. Allouche, L. V. Kemeny, A. L. Hermann, E. M. Roider, N. S. Gray, and D. E. Fisher, "A uv-independent topical small-molecule approach for melanin production in human skin," Cell Reports **19**, 2177–2184 (2017).
37. S. Osseiran, E. M. Roider, H. Wang, Y. Suita, M. Murphy, D. E. Fisher, and C. L. Evans, "Non-euclidean phasor analysis for quantification of oxidative stress in ex vivo human skin exposed to sun filters using fluorescence lifetime imaging microscopy," J. Biomed. Opt. **22**, 125004 (2017).
38. D. Fu, G. Holtom, C. Freudiger, X. Zhang, and X. S. Xie, "Hyperspectral imaging with stimulated raman scattering by chirped femtosecond lasers," The J. Phys. Chem. B **117**, 4634–4640 (2013).
39. E. O. Potma, W. P. de Boeij, P. J. M. van Haastert, and D. A. Wiersma, "Real-time visualization of intracellular hydrodynamics in single living cells," Proc. Natl. Acad. Sci. **98**, 1577–1582 (2001).
40. T. Hellerer, A. M. K. Enejder, and A. Zumbusch, "Spectral focusing: High spectral resolution spectroscopy with broad-bandwidth laser pulses," Appl. Phys. Lett. **85**, 25–27 (2004).
41. W. Langbein, I. Rocha-Mendoza, and P. Borri, "Coherent anti-stokes raman micro-spectroscopy using spectral focusing: theory and experiment," J. Raman Spectrosc. **40**, 800–808 (2009).
42. J. W. Fluhr, M. Gloor, S. Lazzerini, P. Kleesz, R. Grieshaber, and E. Berardesca, "Comparative study of five instruments measuring stratum corneum hydration (corneometer cm 820 and cm 825, skicon 200, nova dpm 9003,

Biomedical Optics EXPRESS

dermalab). part i. in vitro," Ski. Res. Technol. **5**, 161–170 (1999).
43. B. Godin and E. Touitou, "Transdermal skin delivery: Predictions for humans from in vivo, ex vivo and animal models," Adv. Drug Deliv. Rev. **59**, 1152–1161 (2007).
44. J. W. Fluhr, K. R. Feingold, and P. M. Elias, "Transepidermal water loss reflects permeability barrier status: validation in human and rodent in vivo and ex vivo models," Exp. Dermatol. **15**, 483–492 (2006).
45. S. Pfeiffer, G. Vielhaber, J.-P. Vietzke, K.-P. Wittern, U. Hintze, and R. Wepf, "High-pressure freezing provides new information on human epidermis: Simultaneous protein antigen and lamellar lipid structure preservation. study on human epidermis by cryoimmobilization," J. Investig. Dermatol. **114**, 1030–1038 (2000).
46. X. Chen, P. Gasecka, F. Formanek, J.-B. Galey, and H. Rigneault, "In vivo single human sweat gland activity monitoring using coherent anti-stokes raman scattering and two-photon excited autofluorescence microscopy," Br. J. Dermatol. **174**, 803–812 (2016).
47. C. L. Evans, "Nonlinear optical microscopy for melanoma: Challenges, tools and opportunities," Photochem. Photobiol. **94**, 624–632 (2018).
48. I. Saytashev, R. Glenn, G. A. Murashova, S. Osseiran, D. Spence, C. L. Evans, and M. Dantus, "Multiphoton excited hemoglobin fluorescence and third harmonic generation for non-invasive microscopy of stored blood," Biomed. Opt. Express **7**, 3449–3460 (2016).
49. H. Wang, S. Osseiran, V. Igras, A. J. Nichols, E. M. Roider, J. Pruessner, H. Tsao, D. E. Fisher, and C. L. Evans, "In vivo coherent raman imaging of the melanomagenesis-associated pigment pheomelanin," Sci. Reports **6**, 37986 (2016).
50. P. J. Campagnola and L. M. Loew, "Second-harmonic imaging microscopy for visualizing biomolecular arrays in cells, tissues and organisms," Nat. Biotechnol. **21**, 1356–1360 (2003).